Korean J. Chem. Eng., 39(2), 367-376 (2022)
DOI: 10.1007/s11814-021-0903-4

pISSN: 0256-1115
eISSN: 1975-7220

Competitive adsorption of arsenic and mercury on nano-magnetic activated carbons derived from hazelnut shell

Mojtaba Zabihi*, Maryam Omidvar,†, Alireza Motavalizadehkakhky***,****,†, and Rahele Zhiani***,*****

*Department of Chemical Engineering, Neyshabur Branch, Islamic Azad University, Neyshabur, Iran
**Department of Chemical Engineering, Quchan Branch, Islamic Azad University, Quchan, Iran
***Department of Chemistry, Neyshabur Branch, Islamic Azad University, Neyshabur, Iran
****Avdanced Research Center of Chemistry Biochemistry & Nanomaterial, Neyshabur Branch, Islamic Azad University, Neyshabur, Iran
*****New Materials Technology and Processing Research Center, Department of Chemistry, Neyshabur Branch, Islamic Azad University, Neyshabur, Iran
(*Received 11 April 2021 • Revised 22 June 2021 • Accepted 12 July 2021*)

Abstract−Magnetic activated carbons (AC) derived from hazelnut shell using the chemical activation method with $ZnCl_2$ and KOH were prepared in the present work. The adsorption performance of the magnetic sorbents was evaluated for the removal of mercury and arsenic ions in the binary solutions, and the interference of ions with each other during the adsorption process was investigated. The synthesized adsorbents were characterized using XRD, FTIR, BET, XRF, FESEM, TGA and VSM. The XRD results indicated that the small iron oxide crystallites, including goethite and magnetite, were detected on the hazelnut shell-based AC activated by $ZnCl_2$. The extended Langmuir and the modified competitive Langmuir isotherms were applied to fit the competitive adsorption of Hg (II) and As (V) ions using genetic algorithm (GA). The experimental data were in good agreement with the extended Langmuir equation, while the correlation coefficient was measured close to 1. The highest adsorption capacity was calculated to be 80 and 39.31 mg/g for mercury and arsenic ions on the magnetic sample activated by $ZnCl_2$, respectively. The kinetic behavior of carbonaceous adsorbents was studied using pseudo-first and second-order models. The effect of various operating conditions was investigated on the competitive adsorption of metal ions.

Keywords: Competitive Adsorption, Extended Langmuir, Mercury, Arsenic, Activated Carbon, Hazelnut Shell

INTRODUCTION

Heavy metal ions are the most common wastewater pollutants that raise global concern [1,2]. So far, among the several techniques developed for the removal of heavy metal ions from aqueous solutions, adsorption has been the most effective due to its high efficiency, high kinetic rate and low-cost materials [3,4]. Various adsorbents, including porous and non-porous materials, have been applied for adsorption of heavy metal ions from wastewater [5-7]. However, one of the more prominent problems is separation of sorbents from aqueous solutions after the removal of contaminants [8]. The use of membranes [9] and magnetic nanoparticles [10] is the main proposed solution for solving the mentioned problem which has been reported in many studies.

Activated carbons are common adsorbents for treatment of wastewater due to their high surface area, low-cost raw materials, such as agricultural solid wastes and hydrophobicity properties [11,12]. In recent years, many researches have studied the synthesis methods of magnetic nanoparticle supported carbonaceous adsorbents and their capability for adsorption processes. Liu et al. [13] studied the removal of methylene blue cations from aqueous solutions using activated carbon derived by applying potassium hydroxide as the chemical agent. The magnetic nanoparticles were formed on the activated carbon by co-precipitation method for easy separation from solution [14]. Frohlich et al. [15] studied the preparation of magnetic activated carbon by synthesis of nanoparticles of nickel and iron over the substrate using hydrothermal method. The X-ray diffraction results also showed that the nanoparticles of $NiFe_2O_4$ were formed on the activated carbon. The VSM analysis was also carried out to measure the magnetic strength of sample that was calculated to be 41.19 emu/g. Fatehi et al. [8] evaluated the synthesis of magnetic activated carbon derived from almond shell using co-precipitation method under argon atmosphere as an inert gas. So far, many reports have been published on the adsorption of heavy metal ions from the liquid phase, but very few studies have focused on the simultaneous elimination of these harmful ions from aqueous solutions.

The simultaneous presence of heavy metal ions in the industrial wastewater is quite normal, which in the process of adsorption leads to interactions with each other. According to the studies, the simultaneous presence of heavy metal ions in the wastewater might have negative effects on the adsorption performance. Lin et al. [16] empirically investigated the competitive adsorption of Cr (VI) and As (V) on a synthetic magnetic nanoparticle. The results indicated that

†To whom correspondence should be addressed.
E-mail: omidvar_qu@yahoo.com, Amotavalizadeh@yahoo.com

the adsorption capacity of arsenic (V) ions measured much higher in comparison with Cr (VI) and also illustrated a strong interaction between the ions. Cao et al. [17] investigated the competitive adsorption of ions including lead, zinc, copper, cadmium and nickel on an activated carbon prepared using agricultural solid wastes. The results indicated that the highest and lowest adsorption capacity on the synthesized carbonaceous adsorbent was related to lead and zinc ions, respectively. The obtained data also demonstrated that the adsorption capacity was reduced due to the electrostatic interaction between ions. In another study, the adsorption of heavy metal ions in the binary systems on the activated carbon prepared from hard skin of nuts was experimentally investigated [18]. The results showed that the adsorption of copper ions was increased in the binary solutions in the presence of the other metal ions such as nickel, cadmium and zinc. Leus et al. [19] investigated the adsorption process for removal of mercury and arsenic ions on the hematite nanoparticles. The adsorption capacity was calculated to be 16.58 and 102.3 mg/g for mercury and arsenic ions, respectively. Liu et al. [20] also evaluated the competitive adsorption of copper, nickel and cadmium ions on the synthesized absorbent. The results illustrated that simultaneous presence of two metal ions in the aqueous solutions in which interaction between them had a negative effect on the adsorption capacity of the sample. The maximum adsorption capacity measured to be 270 mg/g was related to the adsorption of nickel in the single component system. The adsorption capacity of nickel has been strongly reduced in the presence of other adsorbents, so that the adsorption capacity for nickel was calculated to be 94.34 mg/g.

There are many studies focused on the preparation of activated carbon from hazelnut shell for removal of heavy metal ions from wastewater [3,4,11,12]. In the present study, to extend and develop the previous works, new and modified magnetic activated carbons were prepared from hazelnut shell by chemical agents including $ZnCl_2$ and KOH. The synthesized carbonaceous adsorbents were applied for the simultaneous removal of Hg (II) and As (V) ions in binary solutions. The isotherm of competitive adsorption of mercury and arsenic ions was also evaluated using genetic algorithm to determine the constant parameters of the extended Langmuir and the modified competitive Langmuir equations. Also, the behavior of competitive adsorption was investigated under the various operating parameters.

MATERIALS AND METHODS

1. Preparation of Adsorbent

Iranian hazelnut prepared from the agricultural solid wastes was washed by deionized water for removal of undesirable materials. Then, the raw material was dried in an oven at 100 °C overnight. The dried sample was powdered and screened using mesh no. 40 and 60. The weight ratio of the hard shell of hazelnut and chemical agent ($ZnCl_2$ or KOH) was chosen to be 1 : 1 for impregnation step at 80 °C. The impregnation was carried out to obtain a dark brown solid. After that, the prepared sample was placed in a quartz tube calcined at 500 °C for 1 h under nitrogen flow in a tubular furnace. Then, the prepared activated carbon was screened using mesh no. 100 and 200. As reported in the previous studies, functionalization of activated carbon with carboxyl group increases the dispersion of magnetic nanoparticle on sorbent surface [21]. Therefore, the functionalization was conducted by impregnation with nitric acid at 60 °C for 12 h. The dispersion of magnetic nanoparticles was carried out by co-precipitation method under nitrogen flow. The presence of oxygen during the preparation of magnetic nanoparticles causes to form the hematite phase with a lower magnetic strength in comparison with other iron oxide phases including magnetite and goethite. Briefly, $FeCl_3{\cdot}6H_2O$ and $FeCl_2{\cdot}4H_2O$ according to stoichiometric ratio were dissolved in deionized water at 65 °C for 1 hour. Afterward, the powdered hazelnut shell based activated carbon was added and NaOH solution as a precipitating agent was also added dropwise to set the pH value of the main solution at 10-11. Then, the black sample was separated using the external magnetic field, washed and dried at 100 °C in an oven for 12 h. The samples, including the magnetic activated carbons derived from impregnation of hazelnut shell with KOH and $ZnCl_2$, were named MACK and MACZ, respectively. The non-magnetic activated carbons were also named ACK and ACZ related to the impregnated samples with KOH and $ZnCl_2$, respectively. All the chemical materials used in this work were purchased from Merck (Darmstadt, Germany).

2. Characterization of Carbonaceous Adsorbents

The X-ray diffraction (XRD) patterns for the synthesized magnetic activated carbons were conducted using STOE model D-64295 equipment. XRD test was performed at 30 kV, 20 mA, copper Kα radiation and scanning rate of 3°/min. Fourier transformed infrared spectroscopy (FT-IR, Nicolet IS10) was performed to study the functional groups of sample surface at a resolution of 4 cm^{-1}. Thermogravimetric analysis (TGA) was carried out using TGA-25 apparatus, MettlerToledo Switzerland for evaluating the oxidation resistance of magnetic activated carbons compared with activated carbons. The samples were heated to 1,000 °C, under airflow of 55 ml/min and heating rate of 10 °C/min. The field emission scanning electron microscope (FESEM) was employed to evaluate the morphology of the synthesized samples and to measure the particle size of adsorbents. Therefore, Hitachi equipment (model: S-4160, at 15 kV and vacuum condition) was employed for preparing micro-images. The surface area of the activated carbons and the magnetic samples was measured using nitrogen adsorption-desorption isotherms at 77 K using an ASAP-1100 Micromeritics equipment. The various isotherm theories, including Brunauer-Emmett-Teller (BET) and Barrett-Joyner-Halenda (BJH), were employed for analysis of the obtained data. The pore volume for each sorbent was calculated by the amount of adsorbed nitrogen at relative pressure of 0.99. The chemical elements of magnetic adsorbents and activated carbons were studied by applying X-ray fluorescence (Spectro-Xepos device from Germany). Vibrating sample magnetometer (VSM) was employed to study the magnetic strength of the prepared adsorbents by utilizing LBKFB model (Meghnatis Daghigh, Kavir Co.) equipment at the ambient temperature.

3. Competitive Adsorption Study

Competitive adsorption of mercury and arsenic ions in the aqueous solutions over the magnetic activated carbons named as MACZ and MACK was studied using batch experiments at various operating conditions. Stock solutions of mercury and arsenic ions were

prepared by dissolving the specific amount of $HgCl_2$ and Na_3AsO_4 in deionized water and then diluted to achieve the desired concentration. The adsorption experiments were conducted with 50 mg sample of sorbent and 50 ml of simulated contaminated solution in two conical flasks which were agitated by electrical stirrer at 600 rpm.

The concentration of metal ions was measured by atomic absorption spectrophotometer (Varian, spectra-110-220/880 Australia Pty. Ltd.) equipped with a Zeeman atomizer and the average of three measurements was reported. The adsorption capacity and removal efficiency (Re) of the synthesized samples were calculated using equations below.

$$q_e = \frac{(C_o - C_e)V}{M} \quad (1)$$

$$Re = \frac{C_o - C}{C_o} \times 100 \quad (2)$$

where q_e (mg/g) is the amount of adsorbed metal ions per the amount of adsorbent, C_o and C_e (ppm) are the initial and the equilibrium concentration of heavy metal ions, respectively. V and M are the volume of solutions and the adsorbent dosage, respectively. Genetic algorithm (GA) was employed to determine the constant parameters of the extended Langmuir and the modified competitive Langmuir isotherms as given in Eqs. (3) and (4) [22].

$$q_{ei} = \frac{q_{maxi} b_i C_{ei}}{1 + \Sigma_{j=1}^{N} b_i C_{ei}} \quad (3)$$

$$q_{ei} = \frac{q_i b_i \frac{C_{ei}}{\eta_i}}{1 + \Sigma_{j=1}^{N} b_i \frac{C_{ei}}{\eta_i}} \quad (4)$$

where q_{maxi} and b_i are the maximum capacity of adsorption and the constant parameters of isotherm, respectively. η_i is the interaction factor that indicates the interaction effect of each ions in a multi-component solution. The objective function of GA method for the estimation of constant values of Eqs. (3) and (4) was defined using Eq. (5) which must be minimized:

$$\text{Objective Function} = \Sigma_i \text{abs}\left(\frac{q_{experimental,\,i} - q_{model,\,i}}{q_{experimental,\,i}}\right) \quad (5)$$

where q_{exp} and q_{model} (mg/g) are the obtained adsorption capacity of adsorbents from experimental data and developed models, respectively. The appropriate constant parameters of genetic algorithm including generation size (1000), population size (50), crossover fraction (0.9) and mutation function (Gaussian) were chosen by Matlab software version 2018b.

RESULTS AND DISCUSSION

1. Characterization of Samples

XRD patterns of the magnetic activated carbons (Fig. 1) detected the presence of a cubic magnetite phase at 2θ=35.45° (ICDD=00-001-1111), which may be also ascribed to the presence of tetragonal maghemite (Υ-Fe_2O_3). The peaks with weak intensity at 2θ= 21.33°, 33.66° and 53.21° indicated the presence of orthorhombic

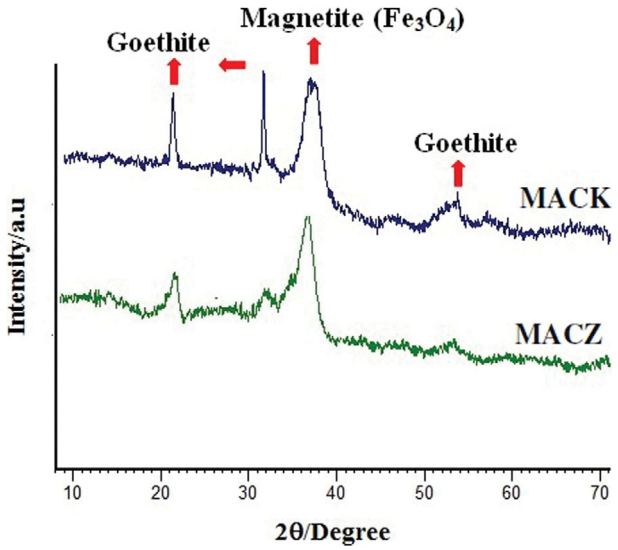

Fig. 1. XRD patterns for the magnetic adsorbents including MACZ and MACK.

Table 1. Calculated the crystallites size of the prepared magnetic activated carbons

Adsorbent	Crystallites size (magnetite)	Crystallites size (goethite)	Crystallites size (Average, nm)
MACZ	32.5	21.3	28.1
MACK	45.8	30.9	37.6

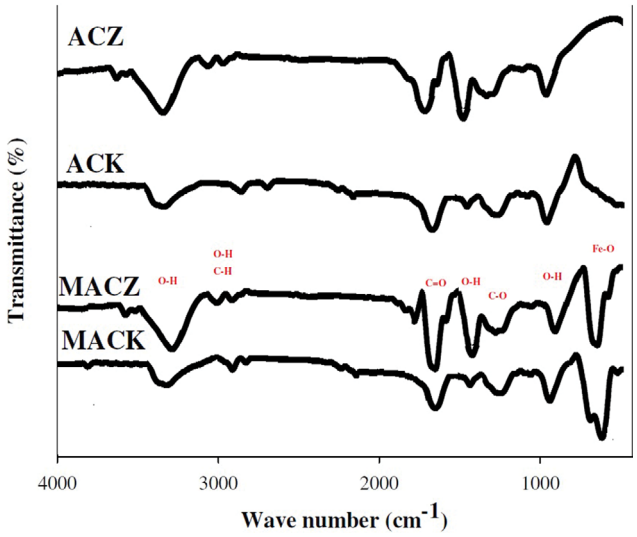

Fig. 2. FTIR graphs for the magnetic and non-magnetic adsorbents including MACZ, MACK, ACZ and ACK.

goethite according to ICDD codes 00-002-0272 and 00-002-0281, respectively. The amorphous phase was also related to the activated carbon in two XRD patterns. The wide and strong peak at 2θ= 35.45° illustrated that small crystallites of magnetite were formed over the two activated carbon samples. The formation of goethite phase over the activated carbons can play an important role for the adsorption of heavy metal ions from aqueous solutions [23]. Based

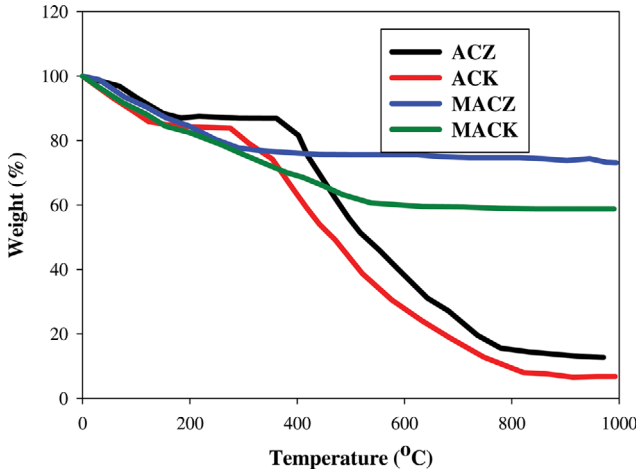

Fig. 3. TGA curves for the magnetic and non-magnetic adsorbents including MACZ, MACK, ACZ and ACK.

on the XRD results, it is expected that the synthesized samples with strong magnetic properties were formed due to the presence of magnetite and goethite crystallites; however, the precipitated crystallites over the MACZ were smaller in comparison with the MACK sample. The size of crystallites of iron oxide over the substrate was calculated using the Scherrer equation [24] and summarized in Table 1. It shows the smaller magnetite crystallites in comparison with goethite.

Fig. 2 illustrates the FTIR graphs of four adsorbents, including ACK, ACZ, MACK and MACZ. The strong characteristic absorption peak at 581.33 cm^{-1} for MACK and MACZ samples can be related to Fe-O bond stretching [8,25] due to the formation of iron oxides over the prepared activated carbons. The broad and strong absorption peak at 2,970 cm^{-1} and 3,500 corresponds to C-H and O-H stretching in carbonyl and phenol groups [26]. It is obvious that the related peak of O-H bond is wider for non-magnetic activated carbons than magnetic samples. Also, the intensity of O-H peaks is higher for the activated carbon which was activated by

Table 2. Textural properties of the magnetic activated carbons

Adsorbent	BET		BJH
	Surface area (m^2g^{-1})	Total pore volume (cm^3g^{-1})	Volume pore (cm^3g^{-1})
ACZ	1,050	0.5264	0.3215
ACK	985	0.4189	0.2958
MACZ	750	0.3033	0.2698
MACK	570	0.2158	0.1998

KOH. The weak peaks at 1,723 and 1,296 cm^{-1} were related to C=O and C-O vibrations, respectively. The existence of grafted carboxylic groups [27] on the activated carbon presented by C=O stretching confirms the successful treatment of substrate using nitric acid through the preparation method.

The thermal behavior of the prepared carbonaceous adsorbents was studied using thermogravimetric analysis (TGA) as seen in Fig. 3. There is a 12% weight loss of activated carbons (ACZ and ACK) related to evaporating the water content of adsorbents at the initial heating stage (0-178 °C). The sharp weight loss of ACZ and ACK occurred in the range of 378-800 °C related to the decomposition of oxygen functional groups. Carbon oxidation at the range of 500-550 °C causes 20% weight loss of activated carbons. The weight of activated carbons was negligibly changed after heating above 800 °C. TGA analysis was also carried out for the magnetic activated carbons, including MACZ and MACK. The results indicated that the weight of MACZ was decreased slowly by heating the adsorbents in the range of 0 to 440 °C. The obtained results also show the decomposition of functional groups, especially carboxylic groups in the range of 186-293 °C. Similar results were achieved for MACK and the weight loss of two prepared magnetic activated carbons was reached to the equilibrium state by heating the sample from 450 to 1,000 °C.

The FESEM images of the magnetic and non-magnetic activated carbons are shown in Fig. 4. The well dispersed morphology of the prepared activated carbons and magnetic adsorbents is

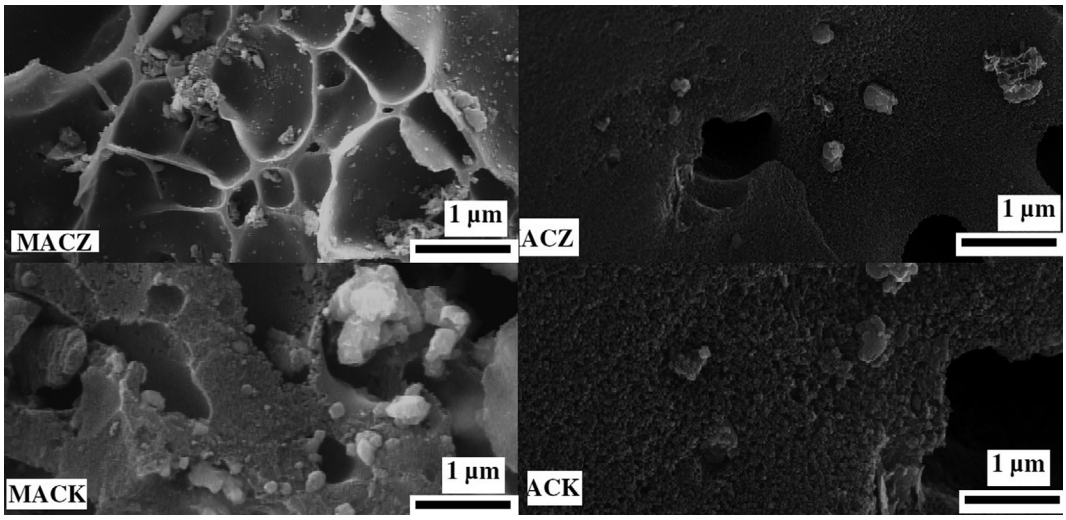

Fig. 4. FESEM micro-images for the magnetic and non-magnetic adsorbents including MACZ, MACK, ACZ and ACK.

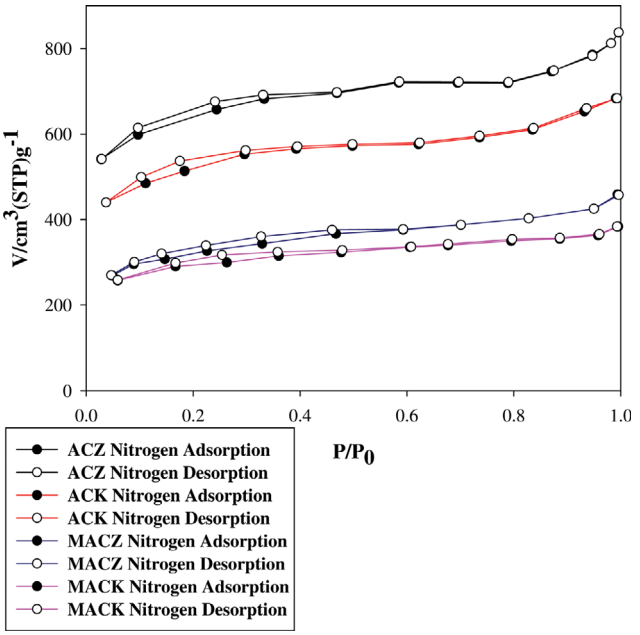

Fig. 5. Nitrogen adsorption-desorption hysteresis for the magnetic and non-magnetic adsorbents including MACZ, MACK, ACZ and ACK.

indicated by the images [28,29]. The porous structure of activated carbons was observed using FESEM images. It was found that chemical activation by KOH and $ZnCl_2$ develops the microporous structure of the samples. Also, between the MACK and MACZ samples, activation by $ZnCl_2$ develops the pore structure of the AC more successfully. This is in agreement with the BET results presented in Table 2. The FESEM results can also confirm the XRD graphs and phases while the iron oxides were formed on the carbonaceous substrate as seen in Fig. 4. The average size of iron oxides was measured by Clemex software between 5 to 200 nm as calculated by Scherrer equation in XRD section.

The porosity and the surface area of the synthesized samples were evaluated using BET analysis. The nitrogen adsorption and desorption isotherms were carried out showing the sharp and mild slope of curves at low and high relative pressures, which are related to the porous structure of samples. According to the FESEM and BET results, it can be confirmed that type IV isotherm is consistent with the morphology of the magnetic and non-magnetic activated carbons as illustrated in Fig. 5. The results show that the structure of activated carbons does not change by dispersing magnetic nanoparticles over the activated carbons. The surface area and pore volume of adsorbents were calculated using BET and BJH theories, respectively. The summarized results in Table 2 indicate that the surface area decreased by dispersing iron oxides, including goethite, magnetite and hematite on the activated carbon due to pore blocking, which is in good agreement with the XRD patterns. The maximum surface area was related to the activated carbon derived by impregnation with $ZnCl_2$ which was 1,050 m^2/g.

The chemical composition of the prepared magnetic adsorbents was measured using XRF analysis, which demonstrated the amount

Table 3. The XRF results of magnetic activated carbons: MACZ and MACK

Chemical element wt%	C	Fe	O	Other element
MACZ	32.97	29.29	27.53	10.21
MACK	35.17	30.79	25.48	8.56

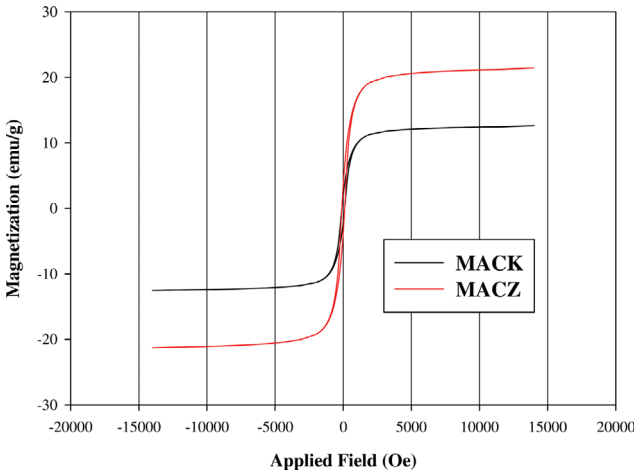

Fig. 6. VSM hysteresis for the magnetic adsorbents including MACZ and MACK.

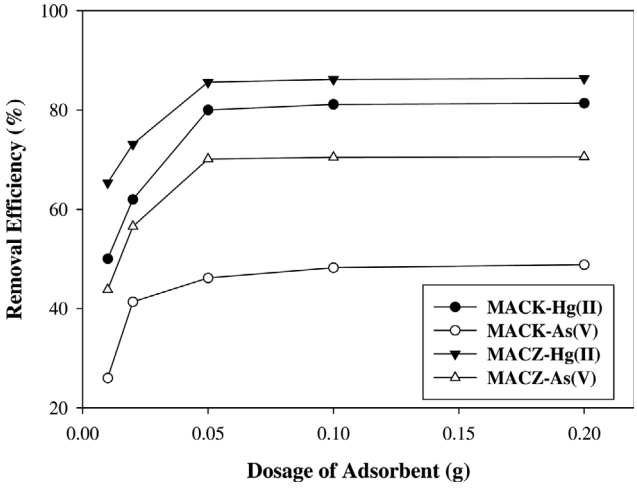

Fig. 7. The effect of adsorbent dosage on the competitive adsorption of mercury and arsenic ions on the MACZ and MACK at 25 °C (Initial concentration=25 ppm, volume of binary solution= 50 mL, pH=6 and contact time=60 min).

of iron over the activated carbon for MACZ and MACK samples as reported in Table 3. The amount of Fe over the hazelnut shell based activated carbons (ACZ and ACK) is in good agreement with the preparation method since it was mentioned that the weight ratio of activated carbon and iron was 1 : 1.

The magnetic strength of MACZ and MACK was studied using VSM analysis, which is plotted in Fig. 6. The highest saturation magnetization values of the magnetic activated carbons were calculated to be 12.63 and 21.48 emu/g for MACK and MACZ, respec-

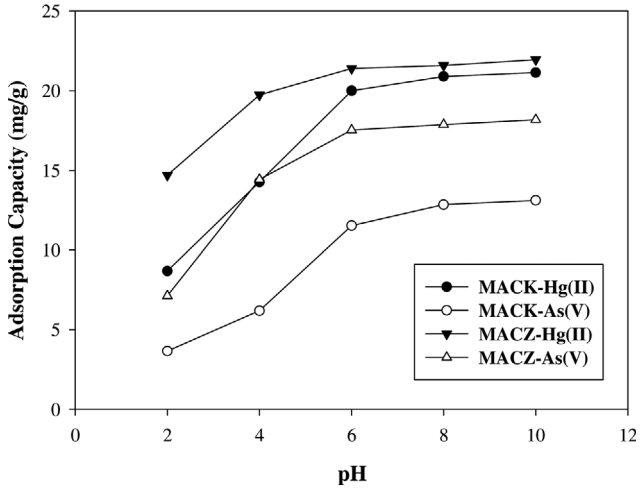

Fig. 8. The effect of pH on the competitive adsorption of mercury and arsenic ions on the MACZ and MACK at 25 °C (Initial concentration=25 ppm, volume of binary solution=50 mL, dosage of adsorbent=50 mg and contact time=60 min).

tively. However, the acceptable magnetic property of the activated carbons confirmed the XRD, BET and XRF results, which indicated the formation of magnetite nanoparticles over the substrates. The VSM results also demonstrated that ACZ can be more suitable substrate for dispersing magnetic particles in comparison with ACK.

2. Effect of Adsorbent Dosage

The effect of adsorbent dosage was studied to find the optimum amount of adsorbent for efficient removal of heavy metal ions. Therefore, the removal efficiency of mercury and arsenic ions in the binary solutions was evaluated at various MACZ and MACK concentrations, while the other operating conditions were kept constant as shown in Fig. 7. The results illustrate that the removal efficiency of the heavy metal ions was increased as increasing the amount of adsorbent from 10 to 50 mg, and after this point the removal efficiency of metal ions achieved an equilibrium level. Therefore, 50 mg of the adsorbents was selected as the optimum value for investigation of adsorption process.

3. Effect of pH on the Competitive Adsorption

Fig. 8 shows the adsorption capacity of the magnetic activated carbons, including MACK and MACZ obtained at various pH values. A significant variation of the adsorption capacity for the prepared adsorbents was observed with increasing pH from 2-6. After this point, negligible enhancement of adsorption capacity was observed. The lower adsorption capacity at low pH can be described by the presence of excess H^+ ions in the solution which had interaction with Hg (II) and As (V) ions for occupying the active sites. This is in agreement with the finding of Yaghmaeian et al. [30] for Hg removal by multi-walled carbon nanotube.

As pH increases, the ions may precipitate by reaction with OH^-. Therefore, the removal efficiency and adsorption capacity will increase apparently. The maximum adsorption capacity of MACK and MACZ was measured to be 21.14, 13.12 and 21.95, 18.19 mg/g at neutral solution for mercury and arsenic ions after 1 h, respectively.

4. Effect of Adsorption Temperature

Figs. 9(a)-9(c) illustrate the effect of adsorption temperature on

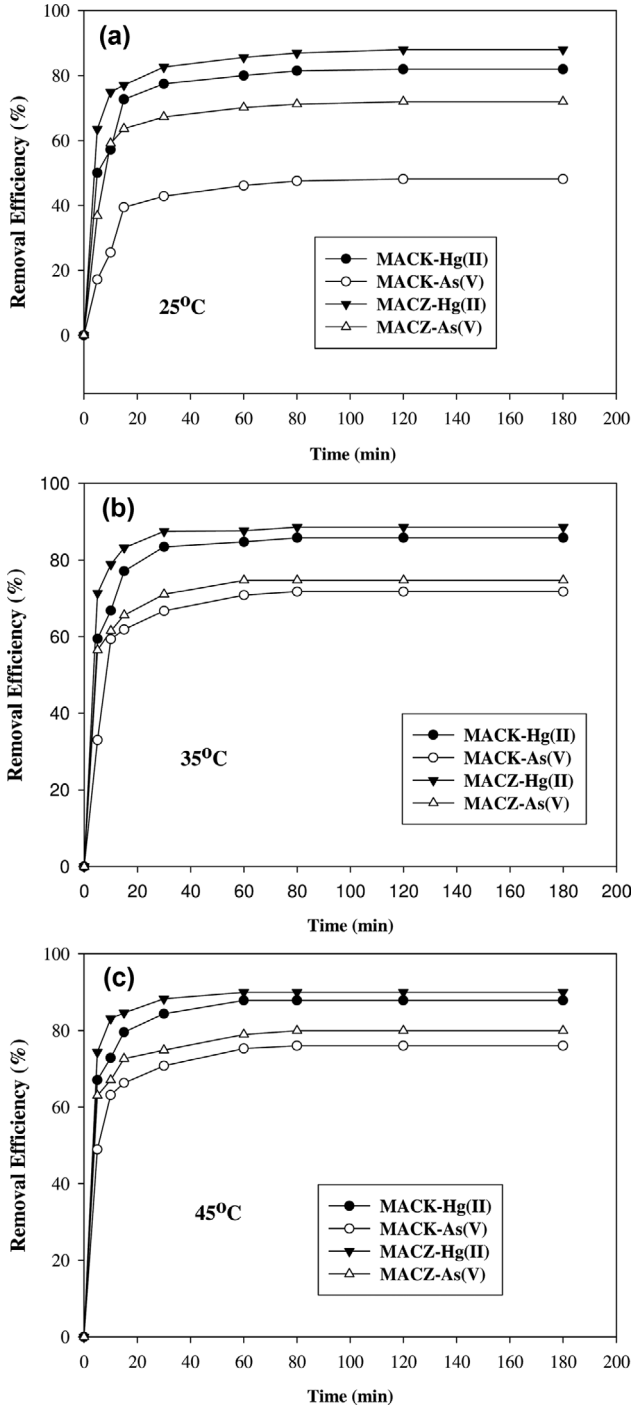

Fig. 9. (a) The effect of temperature (25 °C) and contact time on the competitive adsorption of mercury and arsenic ions on the MACZ and MACK at pH 6 (Initial concentration=25 ppm, volume of binary solution=50 mL and dosage of adsorbent=50 mg). (b) The effect of temperature (35 °C) and contact time on the competitive adsorption of mercury and arsenic ions on the MACZ and MACK at pH 6 (Initial concentration=25 ppm, volume of binary solution=50 mL and dosage of adsorbent=50 mg). (c) The effect of temperature (45 °C) and contact time on the competitive adsorption of mercury and arsenic ions on the MACZ and MACK at pH 6 (Initial concentration=25 ppm, volume of binary solution=50 mL and dosage of adsorbent=50 mg).

Table 4. The constant parameters of kinetic models for MACZ and MACK

Adsorbent-adsorbate	Kinetic model	Constant parameter, K1 (min^{-1}), K2 ($g \cdot mg^{-1} \cdot min^{-1}$)	R^2
MACZ-Hg (II)	Pseudo-first-order	0.00087	0.71320
MACZ- As (V)		0.00130	0.52160
MACK- Hg(II)		0.00130	0.65690
MACK- As (V)		0.00210	0.6652
MACZ-Hg (II)	Pseudo-second-order	0.02080	0.99990
MACZ- As (V)		0.01780	0.99970
MACK- Hg(II)		0.01600	0.99970
MACK- As (V)		0.01160	0.99860

the adsorption capacity during the competitive adsorption of mercury and arsenic ions over the carbonaceous adsorbents. The experimental data show that the adsorption capacity of the prepared samples (MACK and MACZ) for arsenate ions increases with increasing temperature in the range of 25 °C to 45 °C, but maximum adsorption capacity of mercury ions is independent of temperature. The slope of removal efficiency versus time for adsorption of arsenate also rises with increasing the temperature. This may be due to the fact that diffusion plays a significant role in the adsorption over the porous media. Therefore, based on the results, diffusion through the external mass transfer layer and intraparticle diffusion are the main controlling steps of adsorption process [7]. Fig. 9 also indicates the behavior of adsorbents versus the contact time. The adsorption capacity of samples was achieved to the equilibrium level after 60 min from the start of each run. The maximum adsorption capacity was measured to be 89.96 and 79.96 mg/g at 45 °C for mercury and arsenic ions on the MACZ, respectively.

5. Kinetic Study of Adsorption

The kinetic of the simultaneous adsorption of mercury and arsenic ions over the carbonaceous adsorbents was studied using pseudo-first and second-order kinetic models [31]. The linearized form of the kinetic equations was derived to determine the kinetic constant of adsorption as summarized in Table 4. A comparison between the linear forms of each equation with the experimental data is also depicted in Fig. 10. The squared correlation coefficient (R^2) was calculated to be close to one for pseudo-second order kinetic. The results demonstrate that the adsorption of mercury ions was faster over MACZ and MACK in comparison with arsenic ions. The high rate of adsorption also indicates that the adsorbent functional groups enhance the inherent kinetic of adsorption while the diffusion was the slowest step.

$$\mathrm{Log}(q_e - q_t) = \mathrm{Log}q_e - \frac{K_1}{2.303}t \tag{6}$$

$$\frac{t}{q_t} = \frac{1}{K_2 q_e^2} + \frac{t}{q_e} \tag{7}$$

where q_t (mg/g) is the adsorption capacity at time t, q_e is the equilibrium sorption, and K_1 (min^{-1}) and K_2 ($g \cdot mg^{-1} \cdot min^{-1}$) are the constant parameters of pseudo-first and second-order kinetic, respectively.

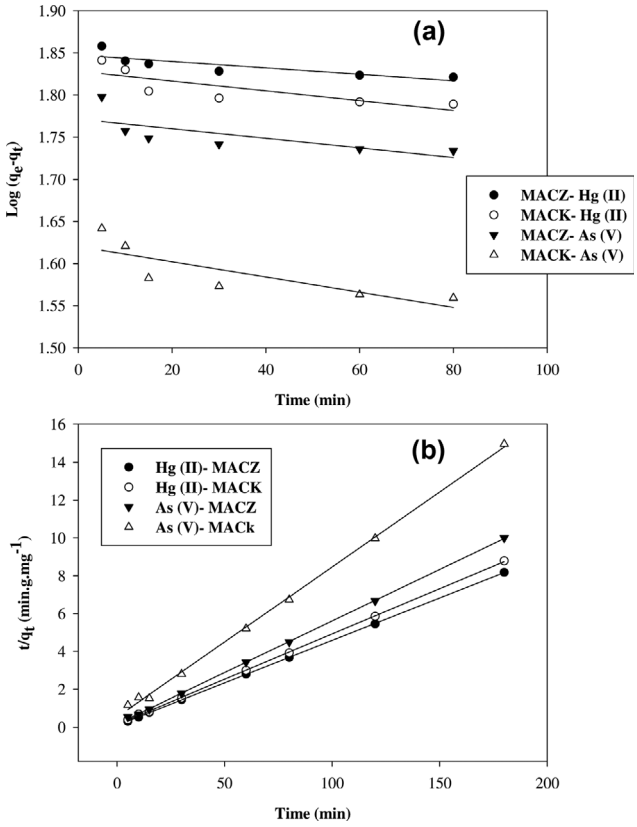

Fig. 10. (a) Pseudo first order kinetic plots for the MACZ and MACK samples at 25 °C. (b) Pseudo second order kinetic plots for the MACZ and MACK samples at 25 °C.

6. Isotherm Models

Competitive adsorption in the binary solution was studied applying two isotherm models for binary solutions. The extended Langmuir model assumes all the active sites are equally reachable for both metal ions and the interaction between the adsorbate species is negligible. On the other hand, the modified competitive Langmuir isotherm is introducing an additional term η in the equation considering the competitive effect of the adsorbates.

Fig. 11 shows the equilibrium adsorption capacity depicted against equilibrium concentration of Hg (II) and As (V) according to the

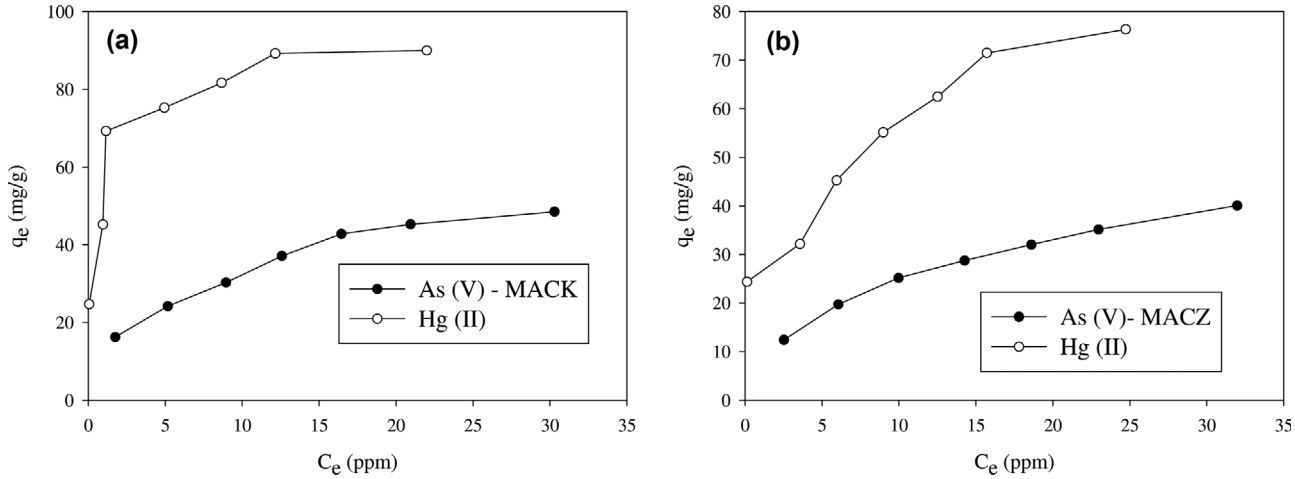

Fig. 11. (a) Adsorption isotherm of mercury and arsenic ions on the MACZ at 25 °C (dosage of adsorbent=10 mg). (b) Adsorption isotherm of mercury and arsenic ions on the MACK at 25 °C (dosage of adsorbent=10 mg).

Table 5. The optimal parameters of binary isotherms for MACZ and MACK

Adsorbent-adsorbate	Isotherm model	q_i (mg/g)	b_i (L/g)	η_i	R^2
MACZ Hg(II)-As(V)	Extended Langmuir	q_{Hg}=80.00	b_{Hg}=0.9971 b_{As}=−0.0856	--	0.9314
		q_{As}=39.31	b_{Hg}=−0.1458 b_{As}=0.3424	--	0.9920
MACK Hg(II)-As(V)	Extended Langmuir	q_{Hg}=69.97	b_{Hg}=0.1825 b_{As}=−0.0425	--	0.9158
		q_{As}=26.40	b_{Hg}=−0.1525 b_{As}=0.2583	--	0.9952
MACZ Hg(II)-As(V)	Modified competitive Langmuir	q_{Hg}=79.99	b_{Hg}=−0.9983 b_{As}=−0.2482	η_{Hg}=−1.0012 η_{As}=2.8977	0.9318
		q_{Hg}=59.33	b_{Hg}=0.000033 b_{As}=0.3772	η_{Hg}=3.03E+4 η_{As}=2.6462	0.9804
MACK Hg(II)-As(V)	Modified competitive Langmuir	q_{Hg}=69.96	b_{Hg}=−0.8112 b_{As}=0.3448	η_{Hg}=−4.4444 η_{As}=−2.8986	09157
		q_{Hg}=49.83	b_{Hg}=0.000052 b_{As}=0.3255	η_{Hg}=1.92E+4 η_{As}=3.0722	0.9913

Table 6. A comparison the performance of adsorbents for competitive adsorption of mercury and arsenic ions

Adsorbent	Heavy metal ions in the multi-component solutions	Adsorption capacity-Hg (II) (mg/g)	Adsorption capacity-As(V) (mg/g)	Ref.
Activated carbon-chemical agent $ZnCl_2$	Zn (II), Hg (II)	66.33	-	[28]
Bentonite-nanocomposite	Pb (II), Hg (II)	12.06	-	[29]
Bentonite-alginate	Pb (II), Hg (II)	66.13	-	[30]
Polyacrylamide/attapulgite	Pb (II), Hg (II)	132.2	-	[31]
Polyacrylamide/attapulgite	Co (II), Hg (II)	138.9	-	[31]
{201} TiO_2	As (V), Flouride	-	36.6	[32]
MACZ	Hg (II), As (V)	80	39.31	This work
MACK	Hg (II), As (V)	69.97	26.40	This work

extended Langmuir equation. As the measured correlation coefficient reported in Table 5, the experimental data are in good agreement with the extended Langmuir model. The calculated constant parameters of the extended Langmuir also show that the presence of arsenic ions in the solutions has negligible effect on the adsorption of mercury ions and the b_i value for arsenic ions were ob-

tained lower compared with mercury ions. The higher adsorption capacity was obtained to be 80 and 39.31 mg/g over MACZ and MACK using the extended Langmuir model. As reported in Table 5, the results extracted from extended Langmuir isotherm are more reliable compared to the modified competitive Langmuir isotherm.

A comparison between different studies for the competitive adsorption of mercury and arsenic ions in the multi-component solutions is presented in Table 6. As summarized in Table 6, there is no published work on the simultaneous adsorption of mercury and arsenic ions in the binary solutions. However, there are some papers that explain the competitive adsorption of mercury and arsenic ions with the other heavy metal ions, for instance Pb (II), Zn (II) and cobalt (II) in multi-component solutions. The results of this study introduce the novel prepared magnetic activated carbons (MACZ and MACK) as the new approach for simultaneous removal of Hg (II) and As (V) ions from aqueous solutions.

CONCLUSIONS

The adsorptive removal of mercury (II) and arsenic (V) ions was investigated using magnetic activated carbons derived from hazelnut shell activated by chemical method. For the binary system of Hg (II) and As (V) ions, the appropriate operating conditions for the maximum adsorption capacity of adsorbents were found at pH 6, adsorbent dose 1 g/L and contact time 1 h. The extracted results from the extended Langmuir equation described the experimental data in comparison with the modified competitive Langmuir equation at equilibrium conditions. The maximum adsorption capacity was calculated to be 80 and 39.31 mg/g for mercury and arsenic on MACZ, and 69.97 and 26.40 mg/g on MACK, respectively. The results indicated that the interaction between mercury and arsenic ions is negligible in the binary mixture, and the presence of arsenic ions in the solutions has a negligible effect on the adsorption of mercury ions. The kinetic of adsorption on the magnetic sorbents follows the second-order kinetic model. The XRD graphs with strong and wide peaks showed that the iron oxide crystallites, including magnetite and goethite, were formed over the activated carbons, which was confirmed by FTIR and VSM methods. The smallest crystallites were sized over the magnetic activated carbon treated by $ZnCl_2$. The higher surface area of MACZ in comparison with MACK is one of the reasons for better performance of this adsorbent for removal of mercury and arsenic ions.

ACKNOWLEDGEMENT

The authors gratefully acknowledge Neyshabur Branch, Islamic Azad University, Neyshabur, Iran.

NOMENCLATURE

C_o : initial concentration of heavy metal ions, ppm
C_e : equilibrium concentration of heavy metal ions, ppm
K_1 : constant parameter of pseudo first order kinetic [min^{-1}]
K_2 : constant parameter of pseudo second order kinetic [$g \cdot mg^{-1} \cdot min^{-1}$]
M : the adsorbent dosage [gr]
q_e : equilibrium adsorption capacity [mg/g]
q_{exp} : experimental adsorption capacity [mg/g]
q_{model} : model adsorption capacity [mg/g]
q_t : adsorption capacity at time t [mg/g]
Re : removal efficiency
V : volume of solutions [L]

REFERENCES

1. M. Marciniak, J. Goscianska, M. Frankowski and R. Pietrzak, *J. Mol. Liq.*, **276**, 630 (2019).
2. M. Sharma, J. Singh, S. Hazra and S. Basu, *Microchem. J.*, **145**, 105 (2019).
3. E. Demirbaş, M. Kobya, S. Öncel and S. Şencan, *Bioresour. Technol.*, **84**(3), 291 (2002).
4. G. Karaçetin, S. Sivrikaya and M. Imamoğlu, *J. Anal. Appl. Pyrol.*, **110**, 270 (2014).
5. A. Ahmadpour, M. Zabihi, M. Tahmasbi and T. R. Bastami, *J. Hazard. Mater.*, **182**(1), 552 (2010).
6. M. Zabihi, A. Ahmadpour and A. H. Asl, *J. Hazard. Mater.*, **167**(1), 230 (2009).
7. M. Zabihi, A. Haghighi Asl and A. Ahmadpour, *J. Hazard. Mater.*, **174**(1), 251 (2010).
8. M. H. Fatehi, J. Shayegan, M. Zabihi and I. Goodarznia, *J. Environ. Chem. Eng.*, **5**(2), 1754 (2017).
9. J. E. Efome, D. Rana, T. Matsuura and C. Q. Lan, *Sci. Total Environ.*, **674**, 355 (2019).
10. V. Nejadshafiee and M. R. Islami, *Mater. Sci. Eng.: C.*, **101**, 42 (2019).
11. Y. Bayrak, Y. Yesiloglu and U. Gecgel, *Micropor. Mesopor. Mater.*, **91**(1), 107 (2006).
12. D. D. Milenković, P. V. Dašić and V. B. Veljković, *Ultrason. Sonochem.*, **16**(4), 557 (2009).
13. Y. Liu, Z. Huo, Z. Song, C. Zhang, D. Ren, H. Zhong and F. Jin, *J. Taiwan Inst. Chem. Engineers*, **96**, 575 (2019).
14. Y. Jiang, Q. Xie, Y. Zhang, C. Geng, B. Yu and J. Chi, *Int. J. Mining Sci. Technol.*, **29**(3), 513 (2019).
15. A. C. Fröhlich, E. L. Foletto and G. L. Dotto, *J. Cleaner Production*, **229**, 828 (2019).
16. S. Lin, C. Lian, M. Xu, W. Zhang, L. Liu and K. Lin, *Appl. Surf. Sci.*, **422**, 675 (2017).
17. F. Cao, C. Lian, J. Yu, H. Yang and S. Lin, *Bioresour. Technol.*, **276**, 211 (2019).
18. I. A. Aguayo-Villarreal, A. Bonilla-Petriciolet and R. Muñiz-Valencia, *J. Mol. Liq.*, **230**, 686 (2017).
19. K. Leus, K. Folens, N. R. Nicomel, J. P. H. Perez, M. Filippousi, M. Meledina, M. M. Dîrtu, S. Turner, G. Van Tendeloo, Y. Garcia and G. Du Laing, *J. Hazard. Mater.*, **353**, 312 (2018).
20. R. Liu and B. Lian, *Sci. Total Environ.*, **659**, 122 (2019).
21. M. Jain, M. Yadav, T. Kohout, M. Lahtinen, V. K. Garg and M. Sillanpää, *Water Res. Ind.*, **20**, 54 (2018).
22. V. K. Rathore, D. K. Dohare, P. Mondal, *J. Environ. Chem. Eng.*, **4**(2), 2417 (2016).
23. C. Qu, M. Ma, W. Chen, P. Cai, X.-Y. Yu, X. Feng and Q. Huang, *Chemosphere*, **193**, 943 (2018).
24. M. Zabihi, F. Khorasheh and J. Shayegan, *RSC Adv.*, **5**(7), 5107

(2015).
25. M. H. Jannat Abadi, S. M. M. Nouri, R. Zhiani, H. D. Heydarzadeh and A. Motavalizadehkakhky, *Int. J. Ind. Chem.*, **10**(4), 291 (2019).
26. K. Fu, Q. Yue, B. Gao, Y. Wang and Q. Li, *Colloids Surf. A: Physicochem. Eng. Aspects*, **529**, 842 (2017).
27. S. Asgari, Z. Fakhari and S. Berijani, *J. Nanostructures*, **4**(1), 55 (2014).
28. S. cheng, L. Zhang, H. Xia, J. Peng, S. Zhang and S. Wang, *J. Porous Mater.*, **22**(6), 1527 (2015).
29. W. Yu, M. Li, X. Ji, Y. Qiu, Y. Zhu and C. Leng, *J. Wuhan Univ. Technol.-Mater Sci. Ed.*, **31**(2), 260 (2016).
30. K. Yaghmaeian, R. Khosravi Mashizi, S. Nasseri, A. H. Mahvi, M. Alimohammadi and S. Nazmara, *J. Environ. Health Sci. Eng.*, **13**(1), 55 (2015).
31. H. Yuh-Shan, *Scientometrics*, **59**(1), 171 (2004).